PROGRESS IN PHOTOVOLTAICS: RESEARCH AND APPLICATIONS, VOL 2, 19–26 (1994)

Research

Optimization of the Rear Contact Pattern of High-efficiency Silicon Solar Cells With and Without Local Back Surface Field

S. Sterk, J. Knobloch and W. Wettling

Fraunhofer-Institut für Solare Energiesysteme, Oltmannsstrasse 5, 79100 Freiburg, Germany

The influence of the point spacing and size on the cell efficiency is studied for different silicon solar cell structures with local rear contacts: the PERC (passivated emitter and rear cell) with its high recombination at the rear contacts and the LBSF (local back surface field) or PERL (passivated emitter and rear locally diffused) cell with reduced combination at the rear contacts due to a diffused high-low junction (or LBSF) beneath the contacts. Float zone materials of different resistivities have been investigated.

The experimental results are explained by three-dimensional finite difference simulations for the open-circuit voltage, the short-circuit current and the fill factor.

INTRODUCTION

High-efficiency silicon solar cells have to be designed carefully in order to minimize all possible losses.[1] Figure 1 shows, as an example, the structure of a PERL (passivated emitter and rear locally diffused) cell,[2] which is also called an LBSF (local back surface field) cell.[3,4] The most important features are: texturized emitter surface in order to reduce reflection losses, a two-step emitter with a shallow and lightly doped region between the front grid lines and a deeper and more heavily doped region under the contacts. Of particular importance are the oxidized surfaces on the front and rear sides. They are only opened for contacts by thin stripes on the emitter side and small holes on the base contact side. The PERL or LBSF cells have, in addition, a locally diffused p^+ area on top of the rear contact dots, which reduces the contact resistivity and acts furthermore as a local back surface field (BSF) for the minority carriers. For the PERC (passivated emitter and rear cell) structure,[5,6] this local BSF is not provided. In this paper, a systematic experimental and theoretical study of the influence of the spacing and the metallization fraction of the rear contact points is presented in order to optimize the cell performance. It will be shown that the PERC-type cell needs a different rear contact pattern from the PERL or LBSF cells.

The reason for this is the high recombination at the rear contacts of PERCs. As a consequence, a high open-circuit voltage V_{oc} and a high short-circuit current I_{sc} require a large point spacing and the minimization of the metallized fraction f_m of the rear surface. On the other hand, this decreases the fill factor FF because of the increased ohmic loss due to current crowding around the contact points. So, the rear contact design with the maximum cell efficiency is a compromise between the separate

1062–7995/94/010019–8 $09.00
© 1994 by John Wiley & Sons, Ltd

Received 27 July 1993
Revised 28 September 1993

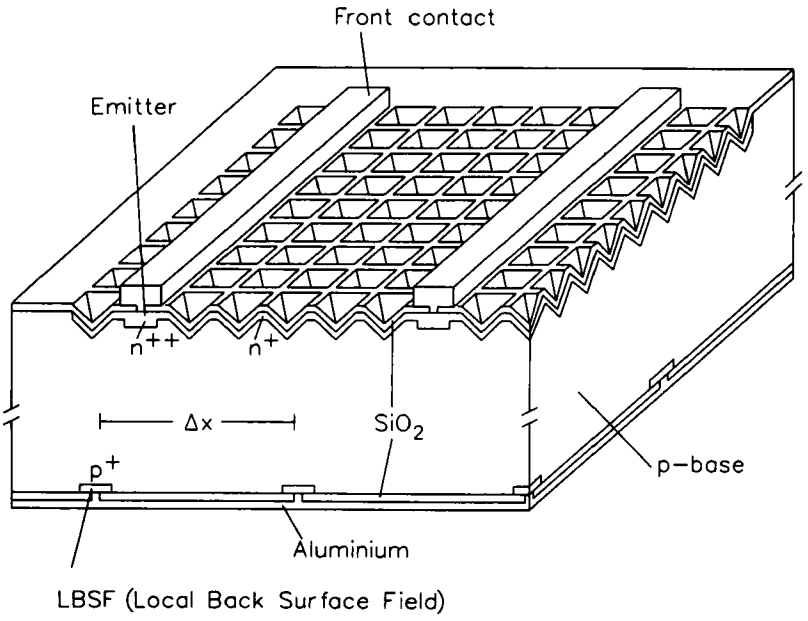

Figure 1. Schematic structure of a PERL or LBSF solar cell

optimization of V_{oc}, I_{sc} and FF. The optimum rear contact design depends strongly on the recombination velocity at the contacts, and is different for different starting materials with different bulk diffusion length and resistivity.

EXPERIMENTAL RESULTS

We processed PERC and LBSF solar cells with different rectilinear rear contact patterns. The process sequence[4] for both cell types is the same except for the additional heavy boron diffusion under the rear contacts of the LBSF cells. The rear contacts have been produced by subeutectic sintering at 450°C for 25 min in forming gas. The point spacing ranged from 250 μm up to 6.6 mm. The rear side metallization fractions have been 0.5 or 4% for the PERCs and 0.5% for the LBSF cells. Additionally, solar cells with a total metallized rear side have been produced as reference cells.

The investigated material was shiny etched 200 μm thick p-type float zone (FZ) silicon with resistivities of 0.25, 0.5 and 1 Ω·cm. We determined the diffusion length of these materials, with photoconductance decay, modulated free carrier infrared absorption and lateral photocurrent measurements,[7] to be about 260, 430 and 660 μm, respectively.

Figures 2 and 3 show the measured solar cell parameters of PERCs. The solar cell parameters are plotted versus the rear contact point spacing. The metallization fraction of the contact points is 4% in Figure 2 and 0.5% in Figure 3. The measurements have been performed on our sun simulator without spectral mismatch corrections. Note that, including this effect, the efficiencies of these cells would be higher by about 0.4% absolute.

First we want to explain the different behaviour of the cells of different resistivity. The 0.25 Ω·cm material shows only a small increase of V_{oc} and I_{sc} with increasing point separation. The reason for this is the low bulk diffusion length of about 260 μm compared to the wafer thickness. The total recombination in the base, which is the sum of the bulk and the rear surface recombination, is dominated by the bulk recombination. Furthermore, the oxide recombination velocity of this material is significantly higher[8,9] than for the materials with higher resistivity. This makes the difference in the effective rear surface recombination (sum of the recombination at the contacts and at the oxide) and therefore the difference

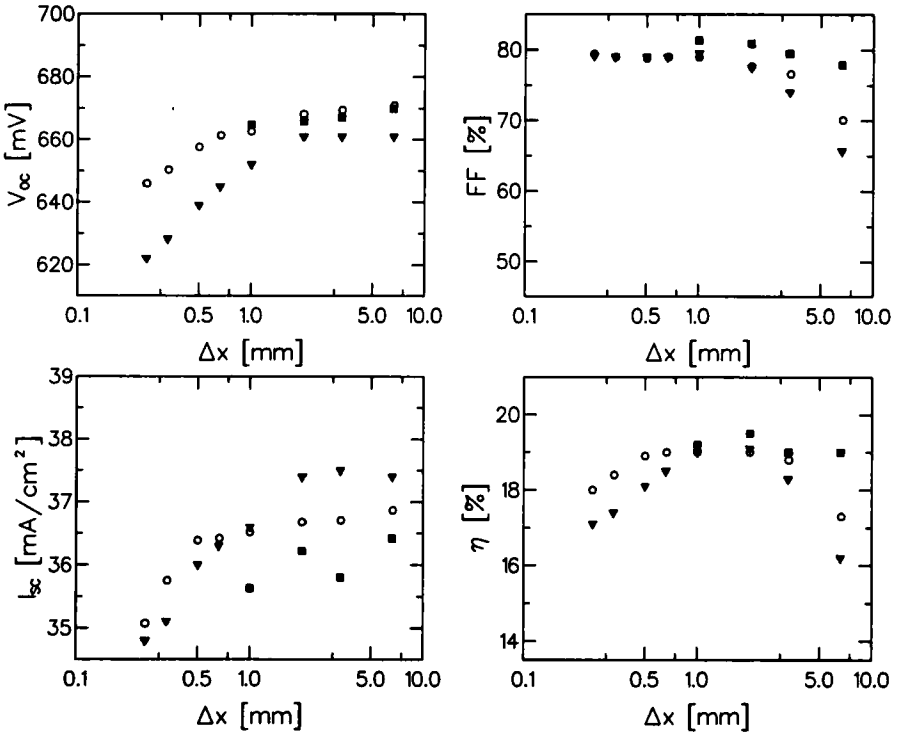

Figure 2. The effect of contact spacing on solar cells without local high-low junction; rear side metallization fraction 4%; bulk resistivity 0.25 (■), 0.5 (○) and 1.0 Ω·cm (▼)

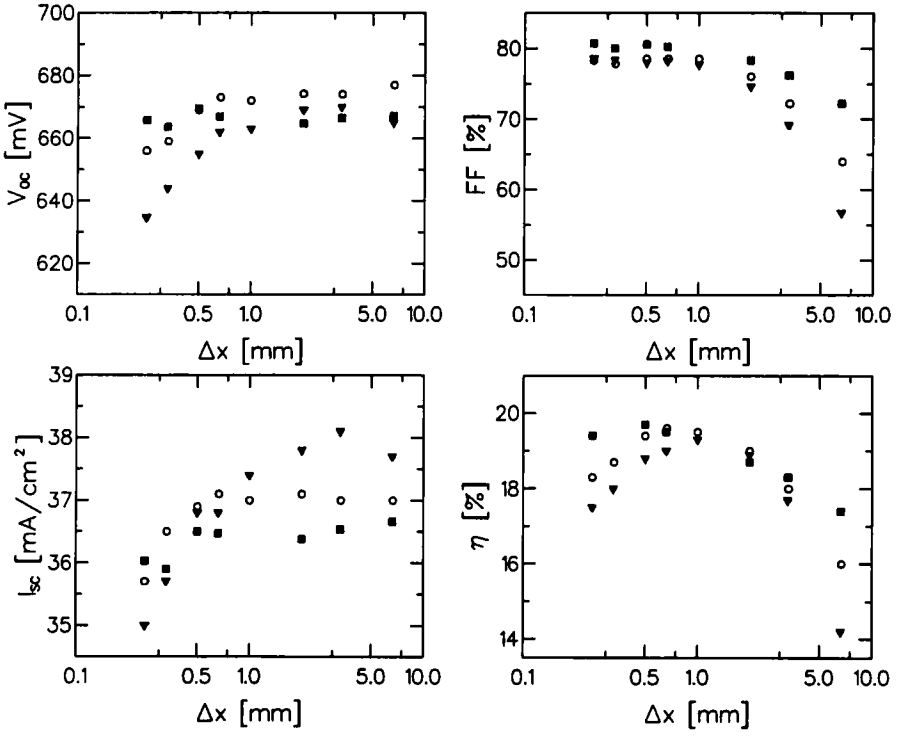

Figure 3. The effect of contact spacing on solar cells without local high-low junction; rear side metallization fraction 0.5%; bulk resistivity 0.25 (■), 0.5 (○) and 1.0 Ω·cm (▼)

in V_{oc} and I_{sc} between the different rear contact designs, smaller. The FF decreases slowly for large point spacings owing to the low resistivity of 0.25 Ω·cm. For these reasons the cell efficiency versus the rear contact point spacing has a broad maximum.

In contrast, the behaviour of the 0.5-Ω·cm and the 1-Ω·cm materials is dominated by the rear surface recombination. The diffusion length of these materials is 430 and 660 μm, respectively. As a consequence, we see a strong increase of V_{oc} and I_{sc} with increasing point spacing but also a faster decrease of FF owing to the higher resistivity. Thus, the efficiency maximum is becoming narrower for higher resistivities.

The minimum and maximum values for V_{oc} and I_{sc} for small and large point spacings can be explained as follows. For the small point spacings, the rear surface acts more and more as a homogeneous surface with a high effective surface recombination velocity S_{eff}, computed as an area-weighted mean of the low oxide and high contact recombination velocity (see next section). If S_{eff} is higher than about 10^5 cm·s^{-1}, then V_{oc} and I_{sc} are close to their values for a cell with an infinite rear surface recombination velocity, i.e. equivalent to a cell with a totally metallized rear surface.

For the smallest point spacing of 250 μm (in Figures 2 and 3), I_{sc} adopts the minimum value (Table I), but the V_{oc} values are still above the minimum value and are different for the two metallization fractions.

In contrast, for a large point spacing the interaction between the metallized and the oxidized regions becomes smaller and the oxidized surface dominates S_{eff} owing to its high area fraction. In this case, V_{oc} and I_{sc} approximate to an area-weighted mean of their values for a totally metallized or a totally oxidized rear surface. For small metallization fractions this value is close to the value for a totally oxidized rear surface.

The comparison of the two different metallization fractions in Figures 2 and 3 shows that for the small metallization fraction in Figure 3, V_{oc} and I_{sc} are significantly higher and increase faster with increasing point spacing. On the other hand, the FFs are lower and decrease faster with increasing point spacing. This opposite behaviour of V_{oc}, I_{sc} and FF is stronger for higher base resistivities. The maximum efficiencies increase about 0.5% absolute with the reduction of the metallization fraction from 4% to 0.5%, and the efficiency maxima shift to smaller point spacings and become sharper. For the PERC process, the lower resistivity materials (0.25 and 0.5 Ω·cm) produce higher efficiencies of about 20% and are less sensitive to the rear contact design of the cell.

Figure 4 shows measured solar cell parameters of LBSF cells for the three resistivities investigated here. The area fraction of the high-low junction (or LBSF) beneath the contact is 1% and the area fraction of rear contacts is 0.5%, as for the cells in Figure 3. Because of the reduced recombination at the contacts, the open-circuit voltage and the short-circuit current values are higher than for the PERCs in Figure 3 and remain unchanged for changing contact point spacing. For small point spacings the efficiency is approximately constant and decreases for large point spacings owing to the reduced FF. The maximum efficiency reached for our LBSF cell is 21.1%[4] on 0.5 Ω·cm material.

Figure 5 shows the long wavelength region of the spectral response measurements for PERCs (eight dotted curves for the eight different investigated point spacings) and for LBSF cells (eight solid curves) on 0.5-Ω·cm material with 0.5% rear side metallization fraction. The solar cell parameters of these cells are shown in Figures 3 and 4. In Figure 5 the contact point spacing varies from 250 μm for the bottom curve up to 6.6 mm for the top curve, for each cell type. The PERCs show a strong increase of the external spectral response in the long wavelength region for increasing point spacing, owing to the

Table I. Measurements of solar cells with totally metallized rear surfaces

Resistivity (Ω cm)	V_{oc} (mV)	I_{sc} (mA cm^{-2})
0.25	645	35
0.5	630	35.2
1.0	610	35.4

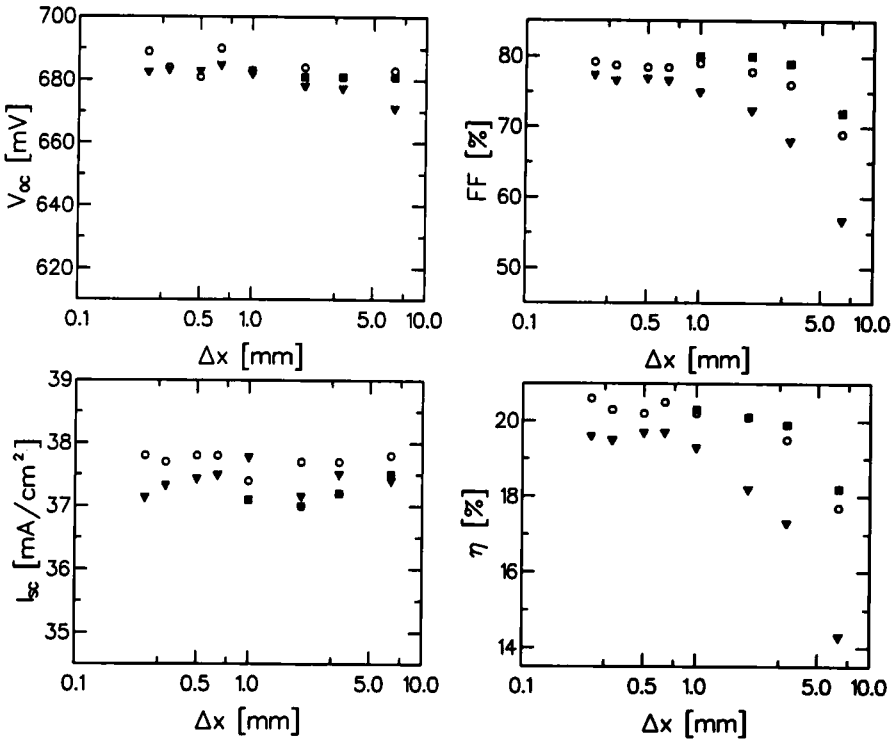

Figure 4. The effect of contact spacing on solar cells with local high-low junction; rear side metallization fraction 0.5%; bulk resistivity 0.25 (■), 0.5 (○) and 1.0 Ω-cm (▼)

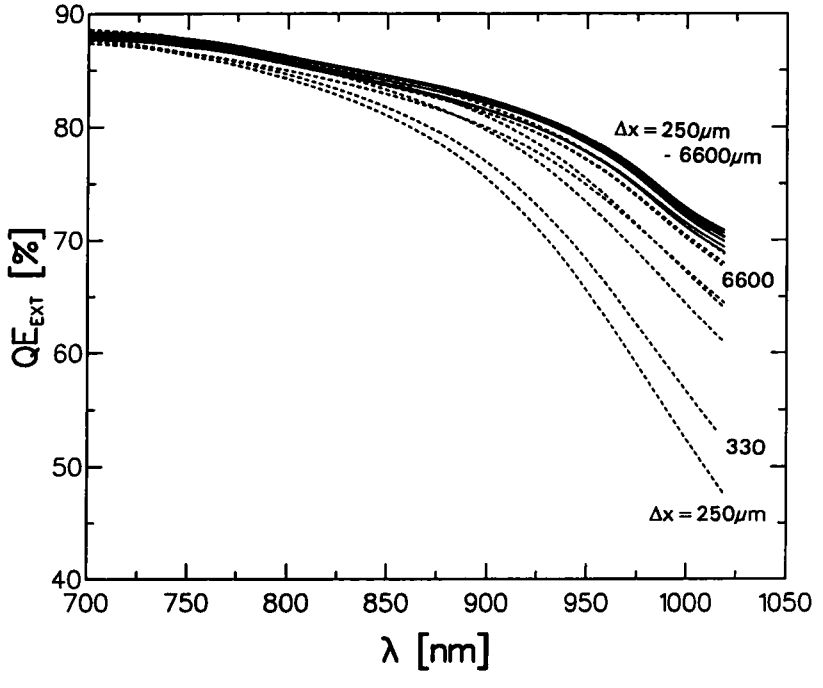

Figure 5. Spectral response measurements of PERCs (dotted curves) and of LBSF cells (solid curves) with different rear contact spacing. Curve parameter Δx = 250, 330, 500 and 660 μm, and 1, 2, 3.3 and 6.6 mm

decreasing effective rear surface recombination. In contrast, the spectral response curves for the LBSF cells remain nearly unchanged for varying point spacing and are therefore difficult to distinguish in Figure 5. Note that they all lie above the curves for the PERCs.

SIMULATIONS

To explain the influence of the rear contact design on the solar cell parameters, we simulated the solar cells with a simple but three-dimensional numerical model based on the finite difference method[10].

The front side texture was neglected. Assuming an ideal conducting and non-recombining emitter, it is sufficient to simulate only the base of the solar cell. Figure 6 shows the simulation region for a rectilinear rear contact pattern. We used a standard Air Mass 1.5 (AM1.5) global solar spectrum with a light intensity of 100 mW cm^{-2}, which is then reduced by the front side reflection and shadowing of about 8.5%. The internal light trapping is taken into account by a back and front side reflectance.

We calculate the open-circuit voltage and the short-circuit current from the three-dimensional diffusion equation for the excess minority carriers, including the photogeneration of excess carriers and a recombination term with a single minority carrier bulk lifetime. Furthermore, we took into account the different surface recombination velocities at the oxidized rear surface and at the contacts. For short-circuit conditions the excess minority carrier density is set to zero at the edge of the depletion region. For open-circuit voltage conditions, the minority carrier density is constant along the edge of the depletion region and the total minority current is zero. The influence of the majority carriers is neglected in this approach. The short-circuit current is calculated as the total minority current at the edge of the depletion region. The open-circuit voltage results from the simulated carrier density at the edge of the depletion region.

The FF has been calculated from simulations of the majority carrier current density at the maximum power point. We assume a maximum FF of 80% for a cell with an ideal conducting base, because of the series resistance in the emitter and the grid fingers. For each rear contact design we compute the FF from this ideal FF and the FF loss due to the simulated series resistance of the base. We assume low injection conditions and neglect the influence of the photogenerated excess charge carriers in our approach. The majority carrier density is set equal to the doping density. Furthermore, we include the specific contact resistivity at the contacts. We solve the three-dimensional Poisson equation for the electrostatic potential in the base and calculate the majority carrier current density from it. At the edge of the depletion region, we assume a constant majority current density. The series resistance of the base is computed from the simulated voltage drop and this current density. The assumption of constant current density at the edge of the depletion region may be a coarse approximation for some cases. However, this affects the calculated base resistance only slightly, because most of the ohmic loss occurs in a small region around the contact points (current crowding).

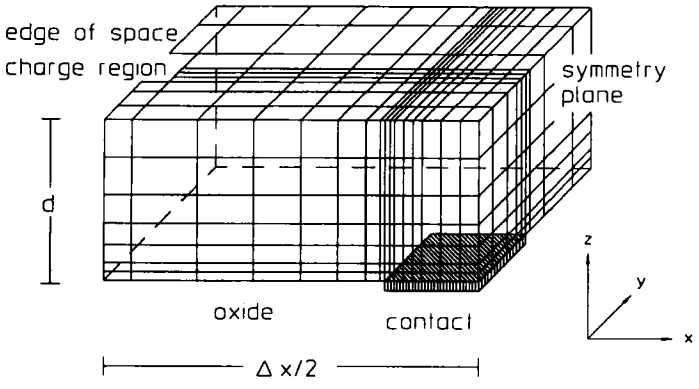

Figure 6. Three-dimensional simulation region

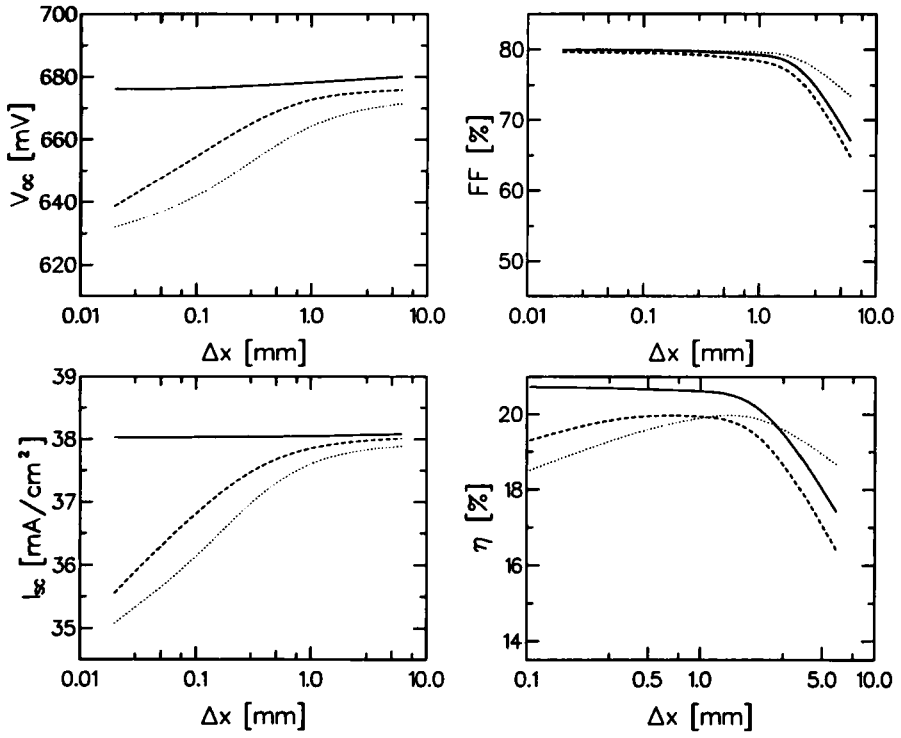

Figure 7. Three-dimensional simulations of PERCs with $f_m = 4\%$ (dotted curves) and $f_m = 0.5\%$ (dashed curves) and of an LBSF cell with $f_m = 0.5\%$ (solid curves)

Figure 7 shows simulations of solar cell parameters. Simulations have been performed of the PERCs of 0.5 Ω·cm, whose experimental results (circles) are given in Figures 2 and 3. The rear side metallization fraction was 4% (dotted line) and 0.5% (dashed line). Simulations have also been performed of LBSF cells (solid line) of 0.5 Ω·cm with a rear side metallization fraction of 0.5%. These values correspond to the experimental values (circles) shown in Figure 4.

We used the following simulation parameters: wafer thickness, 200 μm; bulk resistivity, 0.5 Ω·cm; diffusion length, 500 μm; contact resistivity,[11] 3×10^{-4} or 3×10^{-5} Ω·cm² for PERCs and LBSF cells, respectively; surface recombination velocity at the contacts, infinity or 10^4 cm s^{-1} for the PERCs and LBSF cells, respectively; surface recombination velocity at the oxide, 100 cm s^{-1}.

Comparing the simulations in Figure 7 with the measurements in Figures 2, 3 and 4, we notice that the simulated open-circuit voltage curves explain the difference for different metallization fractions and the dependence on the point spacing for both cell structures. However, the simulated absolute open-circuit values for the LBSF cells are up to 10 mV lower than the measured values. The reason for this may be the oversimplified modelling of the high-low junction as a surface with a low recombination velocity.

For small point spacings the simulated short-circuit currents of the PERCs show a shallower decrease than the measured currents, down to the lower limit of about 35 mA (Table I). This may be due to an increasing surface recombination velocity with decreasing injection level[8,9] for the oxide regions near the contact points. This occurs because of the high recombination at the contact points, which decreases the minority carrier density in these regions. Another possibility is the Dember field effect near the contact point due to current crowding. Both effects are not incorporated in our model but are at present under investigation.

In order to estimate the lower limit (vanishing point spacing $\Delta x \to 0$, vanishing point size but fixed metallization fraction f_m) and upper limit ($\Delta x \to \infty$) of $V_{oc}(\Delta x)$ and $I_{sc}(\Delta x)$ within our three-dimensional diffusion model, we performed simulations for very small ($\Delta x = 1$ μm) and very large point spacing

(Δx = 10 mm) for different parameter sets ($S_m = 10^4$ cm s^{-1} to infinity, S_{ox} = 1–100 cm s^{-1}, f_m = 0.25–4%, L = 250–2000 μm). In both cases we found a good agreement with one-dimensional calculated limit values, using the formulae in Ref. 12.

In between these limits, it is necessary to perform the three-dimesional simulation.[12]

The simulated efficiency curves in Figure 7 show qualitatively the position and height of the relative maxima of the PERCs, as observed in the experimental results. The difference between the simulated and the measured efficiency values for small point spacings is a consequence of the inaccurately simulated short-circuit current. In contrast, the simulations of the LBSF cells agree quite well with the measurements.

SUMMARY

We presented an experimental and theoretical study of the optimization of the rear contact design of the PERC and the PERL or LBSF cell structures. The theoretical study was based on three-dimensional finite difference simulations of the base of the solar cell. The calculations describe the cell performance quite well. We showed that the efficiency of the simple PERC structure depends strongly on the rear contact design. We get the highest efficiencies for PERCs using substrates of low resistivity, e.g. 0.25 and 0.5 Ω·cm. For the optimum design for each of these resistivities, we reached an efficiency of about 20%, which is only 1% less than for our LBSF cells.

The LBSF cells are less sensitive to the rear contact point spacing. We obtained the highest efficiency of 21.1% for 0.5 Ω·cm material with a small rear contact spacing.

Acknowledgements

This work was supported by the German Federal Ministry for Research and Technology. We wish to thank our clean room team—A. Noel, U. Schubert, F. J. Kamerewerd and C. Faller—for processing the solar cells, E. Schäffer for the measurements and Dr A. B. Sproul for useful discussions.

REFERENCES

1. M. A. Green, *High Efficiency Silicon Solar Cells*, Trans Tech Publications, Switzerland, 1987.
2. A. Wang, J. Zhao and M. A. Green, '24% Efficient silicon solar cell', *J. Appl. Phys. Lett.*, **57**, 602–604 (1990).
3. J. Knobloch, A. Aberle and B. Voss, 'Cost effective processes for silicon solar cells with high performance', *Proc. 9th E.C. PVSEC*, September 1989, pp. 777–780.
4. J. Knobloch, A. Noel, E. Schäffer, U. Schubert, F. J. Kamerewerd, S. Klußmann and W. Wettling, 'High efficiency solar cells from FZ, CZ and MC silicon material', *Proc. 23rd IEEE PVSC*, Louisville, KY, May 1993.
5. A. W. Blakers, A. Wang, A. M. Milne, J. Zhao, X. Dai and M. A. Green, '22.6% Efficient silicon solar cells', *Proc. 4th Int. PVSEC*, Sydney, February 1989, pp. 801–806.
6. M. A. Green, A. W. Bakers, J. Zhao, A. M. Milne, A. Wang and X. Dai, 'Characterization of 23-percent efficient silicon solar cells', *IEEE Trans. Electron Devices* **37**(2), 331–336 (1990).
7. S. Sterk, 'Determination of the bulk diffusion length by lateral photocurrent measurements', to be published.
8. A. Aberle, S. Glunz and W. Warta, 'Impact of illumination level and oxide parameters on SRH recombination at the Si–SiO_2 interface', *J. Appl. Phys.* **71**(9), 4422 (1992).
9. S. Glunz, A. Sproul, W. Warta and W. Wettling, 'Injection level dependent recombination velocities at the Si–SiO_2 interface for various dopant concentrations', accepted for publication *J. Appl. Phys.*, February 1994.
10. S. Selberherr, *Analysis and Simulation of Semiconductor Devices*, Springer-Verlag, Vienna, 1984.
11. D. L. Meier and D. K. Schroder, 'Contact resistance: its measurement and relative importance to power loss in a solar cell', *IEEE Trans. Electron Devices* **31**(5), 647–653 (1984).
12. M. Schöfthaler, U. Rau and J. H. Werner, 'Optimization of the back contact geometry for high efficiency solar cells', *Proc. 23rd IEEE PVSC*, Louisville, KY, May 1993.